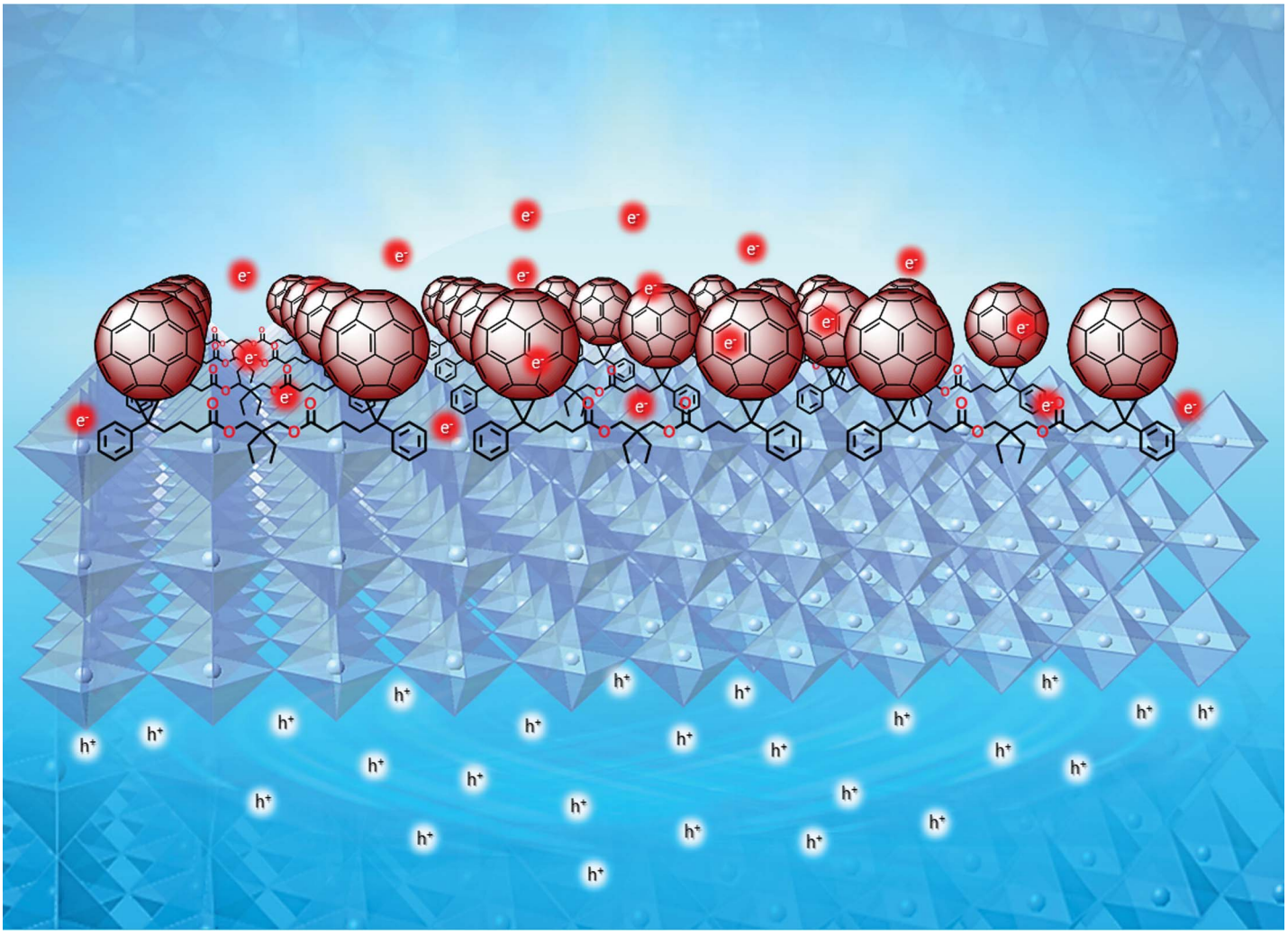

Showcasing research from the group of Luis Echegoyen, Carbon Nanomaterials Laboratory, University of Texas at El Paso.

A dimeric fullerene derivative for efficient inverted planar perovskite solar cells with improved stability

Fullerene derivatives can efficiently passivate the interfacial defects of perovskite layers to improve the performance of perovskite solar cells (PSCs). Here, a new dimeric fullerene derivative D-C60 was synthesized and used as an Electron Transporting Material in PSCs.

As featured in:

See Luis Echegoyen *et al.*, *J. Mater. Chem. A*, 2017, **5**, 7326.

ROYAL SOCIETY OF CHEMISTRY

rsc.li/materials-a

Registered charity number: 207890

Journal of Materials Chemistry A

PAPER

View Article Online
View Journal | View Issue

Cite this: J. Mater. Chem. A, 2017, 5, 7326

A dimeric fullerene derivative for efficient inverted planar perovskite solar cells with improved stability†

Chengbo Tian,[a] Kevin Kochiss,[c] Edison Castro,[a] German Betancourt-Solis,[a] Hongwei Han[b] and Luis Echegoyen*[a]

Received 11th January 2017
Accepted 22nd February 2017

DOI: 10.1039/c7ta00362e

rsc.li/materials-a

Fullerene derivatives can efficiently passivate the interfacial defects of perovskite layers to improve the performance of perovskite solar cells. In this work, a new dimeric fullerene derivative (D-C_{60}) with two [6,6]-phenyl-C_{61}-butyric acid methyl ester ($PC_{61}BM$) units was designed, synthesized and applied as the electron transporting material (ETM) in perovskite solar cells (PSCs) taking advantage of its appropriate energy levels, relatively fast electron mobility, and easy solution processability compared to the widely used $PC_{61}BM$, D-C_{60} can efficiently passivate the trap states between the perovskite and fullerene layers, leading to improved electron extraction and overall photovoltaic performance. Devices based on D-C_{60} as the ETM achieved power conversion efficiencies (PCEs) of 16.6%, which is significantly higher than that observed with $PC_{61}BM$ (14.7%). In addition, the more hydrophobic and compact D-C_{60} layer resulted in higher device stability than that with $PC_{61}BM$. These results show that covalently linked dimeric fullerene derivative can act as efficient electron transporting materials (ETMs) for high performance PSCs.

1. Introduction

The unique properties of organic–inorganic hybrid perovskite materials (typically $CH_3NH_3PbI_3$), such as high light absorption coefficients,[1,2] long carrier diffusion lengths,[3–5] high electron/hole mobilities,[6] simple device architectures, low-temperature fabrication processes,[7] compatibility with flexible substrates,[8,9] negligible hysteric behavior,[10] and efficiencies comparable to those of commercial standards,[11] make them promising candidates for the development of the next-generation photovoltaic solar cells for commercial applications. Currently, PSCs are the most rapidly developing class, with certified efficiencies rising from 3.8% in 2009 to 22.1% in 2016.[1,12]

In inverted planar PSCs, the perovskite layer is surrounded by an electron transporting layer (ETL) and a hole transporting layer (HTL). The HTL, PEDOT:PSS or NiOx,[8,13] is connected to the anode, ITO or FTO, while the ETL is typically a fullerene derivative that is in direct contact with the metal cathode, Al.

$PC_{61}BM$ is the most widely used fullerene derivative in photovoltaic applications, and has become the standard in the field, due to its efficient electron transporting and solution processable properties.[14,15]

In 2013, Jeng and co-workers reported a PCE of 3.9% for inverted planar PSCs using $PC_{61}BM$ as the ETM. The reasonable efficiency of this type of devices demonstrated that fullerene derivatives were promising ETMs in PSCs.[16] Recently, Nie and Im's group reported a device with an efficiency of 18% by developing a new perovskite deposition technique.[17,18] Huang's group recently obtained a remarkable efficiency, as high as 19.4%, which is comparable to those of mesoporous perovskite solar cells, by means of a simple solvent annealing process to improve the surface of the perovskite, resulting in a better electron extraction into the fullerene layer.[19]

To explore the effect of functional groups on the performance of fullerene-based PSCs, double fullerene layers or fullerene derivatives with different functional groups have been studied.[20–27] However, up to now, all of the fullerene derivatives reported in PSCs are monomeric derivatives and to the best of our knowledge, dimeric fullerene derivatives as ETMs in PSCs have never been explored. There is a limited number of dimeric fullerene derivatives that were investigated in polymer solar cells.[28,29] Due to the excellent performance of $PC_{61}BM$-based PSCs,[30] a dimeric fullerene with two $PC_{61}BM$ units was expected to show improved performance in PSCs.

Herein, we report the synthesis, characterization and photovoltaic properties of a fullerene dimer derivative (D-C_{60}), the structure of which is shown in Scheme 1. Due to suitable energy levels and adequate electron mobility of D-C_{60}, the best efficiency obtained from a device based on this compound was

[a]Department of Chemistry, University of Texas at El Paso, 500 West University Avenue, El Paso, TX 79968, USA. E-mail: echegoyen@utep.edu

[b]Michael Grätzel Center for Mesoscopic Solar Cells, Wuhan National Laboratory for Optoelectronics, School of Optical and Electronic Information, Huazhong University of Science and Technology, Wuhan 430074, Hubei, People's Republic of China

[c]Department of Chemistry and Biochemistry, Center for Polymers and Organic Solids, University of California, Santa Barbara, CA 93106, USA

† Electronic supplementary information (ESI) available. See DOI: 10.1039/c7ta00362e

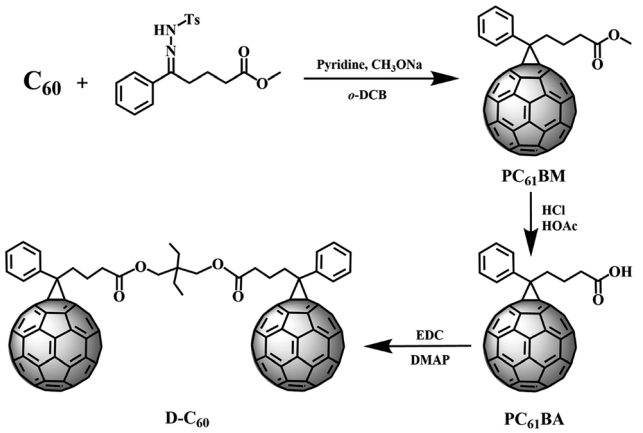

Scheme 1 Synthesis of D-C_{60}.

16.6%. This value was higher than that for the analogous $PC_{61}BM$ based PSCs, 14.7%. Meanwhile, the higher hydrophobicity of D-C_{60} compared to that of $PC_{61}BM$ resulted in better device stability.

2. Experimental and methods

Materials synthesis

[6,6]-Phenyl-C_{61}-butyric acid ($PC_{61}BA$) was synthesized by following previously reported procedures.[31] The synthetic procedure followed to prepare (D-C_{60}) is presented in Scheme 1. EDC (25.6 mg, 0.13 mmol) was added slowly to a pre-cooled solution of 2,2-diethyl-1,3-propanediol (6.6 mg, 0.05 mmol), $PC_{61}BA$ (100.0 mg, 0.11 mmol), and a small amount of DMAP in 40 mL of dry dichloromethane. The mixture was stirred for 36 h at room temperature. After drying under vacuum, the residual mixture was purified by silica gel column chromatography (toluene as eluent). D-C_{60} was precipitated from methanol as a dark-brown solid. ^{1}H NMR ($CDCl_3$, 400 MHz) (Fig. S1†): δ (ppm) 0.88 (6H, t, $J = 5.16$ Hz), 1.42 (4H, m), 2.19 (4H, m), 2.53 (4H, t, $J = 7.52$ Hz), 2.91 (4H, m), 3.68 (4H, s), 7.47 (2H, t, $J = 7.32$ Hz), 7.55 (4H, t, $J = 7.46$ Hz), 7.93 (4H, d, $J = 7.52$ Hz). ^{13}C NMR ($CDCl_3$, 100 MHz) (Fig. S2†): δ (ppm) 173.48, 148.80, 147.81, 145.85, 145.19, 145.15, 145.08, 145.03, 144.79, 144.66, 144.50, 144.42, 144.01, 143.76, 143.12, 143.03, 142.99, 142.93, 142.23, 142.18, 142.13, 142.11, 140.99, 140.75, 138.03, 137.57, 136.73, 132.09, 128.44, 128.24, 79.86, 51.85, 51.68, 33.88, 33.67, 29.70, 22.37. MALDI-TOF-MS m/z: calcd 1888.3, found 1888.6.

Device fabrication

Methylammonium iodide (CH_3NH_3I) was prepared using a previously reported procedure.[32] PSCs with a configuration of FTO/PEDOT:PSS/$CH_3NH_3PbI_3$/$PC_{61}BM$ (or D-C_{60})/Al were fabricated on FTO-coated glass substrates with a resistivity of 10 Ω cm^{-2}. The patterned FTO glass substrates were cleaned sequentially with detergent, deionized water, and ethanol, each step for 15 min dried with nitrogen gas and finally treated in a UV-ozone oven for 20 min. After passing through a 0.45 μm PVDF filter, the PEDOT:PSS solution (Baytron P VP AI 4083) was spin-coated onto the treated FTO substrates at 5000 rpm for 30 s, and heated at 150 °C for 15 min in air. Then a solution of 1 M PbI_2 in DMF was spin-coated at 3000 rpm for 30 s on top of the PEDOT:PSS coated substrates, and dried on a hot plate at 70 °C for 10 min. The FTO/PEDOT:PSS/PbI_2 substrates were then transferred to a vacuum oven to be converted to $CH_3NH_3PbI_3$ by means of a vapor-assisted gas–solid crystallization process following previously reported methods.[27,33] After the $CH_3NH_3PbI_3$ films were formed and then cooled to room temperature, 2 wt% $PC_{61}BM$ (or D-C_{60}) dissolved in chlorobenzene was spin-coated onto the $CH_3NH_3PbI_3$ layer at 1200 rpm for 30 s. To complete the devices, aluminum electrodes (100 nm) were deposited by thermal evaporation under a pressure of 2×10^{-6} Torr through a shadow mask. The active area of the devices was determined by a mask with an aperture in the middle (7 mm^2).

Device characterization

The current–voltage (J–V) characteristics of photovoltaic cells were tested using a Keithley 2420 source measure unit under a Photo Emission Tech SS100 Solar Simulator, and the light intensity was calibrated by a standard Si solar cell. The external quantum efficiencies (EQEs) were measured using a Bentham (from Bentham Instruments Ltd) measurement system. The light intensity was calibrated using a single-crystal Si photovoltaic cell as the reference. The J–V and EQE measurements were carried out in air. The SEM images were collected using a ZEISS Sigma FE-SEM, where the electron beam was accelerated in the range of 500 V to 30 kV. Film thicknesses were measured using a KLA Tencor profilometer. The contact angles of water were determined using a Ramé-Hart model 250 goniometer using pure deionized water at room temperature at a constant volume of 5 μL. A total of ten static measurements were analyzed and averaged for each ETM layer. The steady photoluminescence (PL) spectra were obtained using an Edinburgh instruments FLS980 fluorescence spectrometer.

3. Results and discussion

The synthetic approach to prepare D-C_{60} is presented in Scheme 1. In this approach the two fullerenes are linked by an alkyl bridge between the ester functional groups on the $PC_{61}BM$s. D-C_{60} exhibits a slightly higher lowest unoccupied molecular orbital (LUMO) energy level than the mono-adduct fullerene derivatives,[30] making it a good candidate to act as the ETM in PSCs. 2,2-Diethyl-1,3-propanediol was used to connect the two $PC_{61}BM$ units in order to increase the solubility of the dimer and to result in a homogeneous and compact film, with high hydrophobicity to improve water inclusion and enhance the device stability.

$PC_{61}BM$ (99%) was bought from Nano-C. $PC_{61}BA$ was synthesized heating $PC_{61}BM$ and hydrochloric acid under reflux in toluene for 12 h. D-C_{60} was obtained from the reaction of $PC_{61}BA$ with 2,2-diethyl-1,3-propanediol in anhydrous dichloromethane. The final product was characterized by MALDI-TOF mass spectrometry, ^{1}H and ^{13}C NMR (see ESI†).

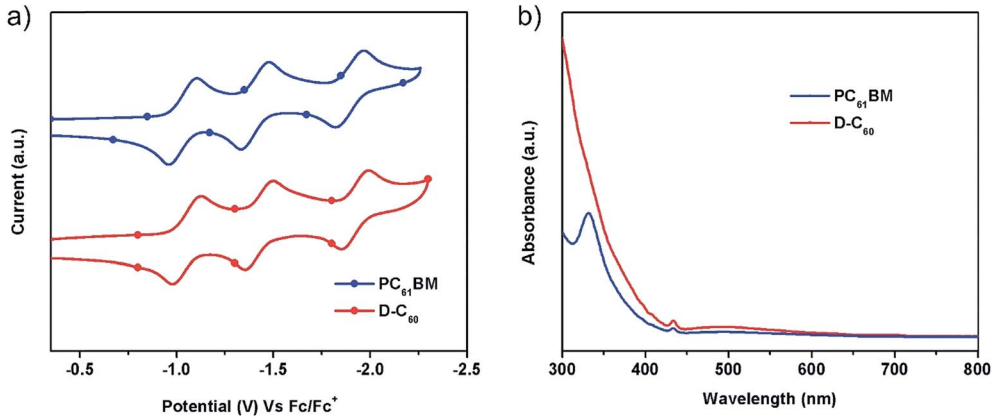

Fig. 1 (a) Cyclic voltammetric scans for D-C_{60} and $PC_{61}BM$ at a scan rate of 100 mV s^{-1}. (b) UV-vis absorption spectra of D-C_{60} and $PC_{61}BM$ in toluene solution.

Due to the flexible connecting group, D-C_{60} exhibits excellent solubility in normal organic solvents such as dichloromethane, chloroform, and chlorobenzene, which makes it suitable for solution-processed PSCs.

The energy levels of fullerene derivatives are important to assess their electron extraction and hole blocking properties in PSCs. The electrochemical properties of $PC_{61}BM$ and D-C_{60} were studied *via* cyclic voltammetry (CV) in the range of 0 to −2.0 V *vs.* Fc/Fc^+. Both exhibit three independent well-defined reversible reduction waves (see Fig. 1a and S3†). The half-wave potentials for the reduction processes are listed in Table S1.† The LUMO energy levels of the compounds were calculated from their onset reduction potentials (E_{red}^{on}) using the equation; LUMO energy level = $-e(E_{red}^{on} + 4.80)$ (eV).[34] These values are listed in Table 1. The LUMO energy levels were estimated at −3.88 and −3.90 eV for D-C_{60} and $PC_{61}BM$ respectively, which are similar to previous reports.[29] These values indicate that both compounds can be used as efficient ETMs in PSCs.

Based on their maximum absorption onsets, as shown in Fig. 1b and Table 1, and the values of the LUMO energy levels, D-C_{60} and $PC_{61}BM$ were estimated to have HOMO values of −5.61 and −5.63 eV, respectively, deep enough to block holes.

For PSC devices, photovoltaic performance is heavily influenced by the carrier mobilities of the charge transporting layers. High electron mobility of the fullerene derivatives improves the short-circuit current density (J_{sc}) and thus the PCEs. The electron mobility of D-C_{60} and $PC_{61}BM$ were measured by the space-charge limited current (SCLC) method (Fig. S4†) and the Mott–Gurney law,[35] based on electron-only devices with the structure ITO/Cs_2CO_3/fullerene derivative/Ca/Al, and found to be 9.83×10^{-4} and 6.85×10^{-4} cm^2 V^{-1} s^{-1}, respectively. The higher electron mobility of D-C_{60} suggests that the fullerene cages are better packed for D-C_{60} than for $PC_{61}BM$. The higher electron mobility of D-C_{60} leads to a higher short-circuit current density and PCE than that of $PC_{61}BM$-based PSC devices.

To test the performance of D-C_{60} as the ETM in PSCs, planar structure devices were prepared, as shown in Fig. 2a, with a configuration: FTO/PEDOT:PSS/$CH_3NH_3PbI_3$/$PC_{61}BM$ (or D-C_{60})/Al. The energy-level alignment of all materials involved in the device is shown in Fig. 2b. The perovskite layer of the device was prepared by a vapor-assisted gas–solid crystallization process, previous reported.[33] After this process, the perovskite layer on PEDOT:PSS, as shown in Fig. 2c, exhibits homogeneous and well packed grains with no pinholes. As shown in the cross-section of the device (Fig. 2d), excellent contact results between the perovskite and the fullerene layers. The thickness of each layer was measured using a profilometer, showing that the

Table 1 Electrochemical and photo-physical data of D-C_{60} and $PC_{61}BM$

Compound	λ_{abs} (nm)	E_g (eV)	E_{red}^{on} (V)	LUMO (eV)	HOMO (eV)
D-C_{60}	717	1.73	0.92	−3.88	−5.61
$PC_{61}BM$	718	1.73	0.90	−3.90	−5.63

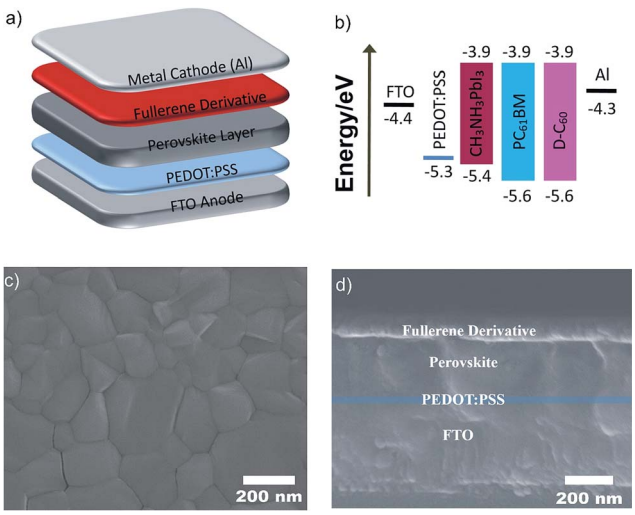

Fig. 2 (a) Configuration scheme of the inverted structure planar perovskite solar cells, (b) energy level diagram of the materials used in PSCs, (c) top-view SEM image of the perovskite film, and (d) cross-sectional SEM image of the device FTO/PEDOT:PSS/perovskite/fullerene derivative film.

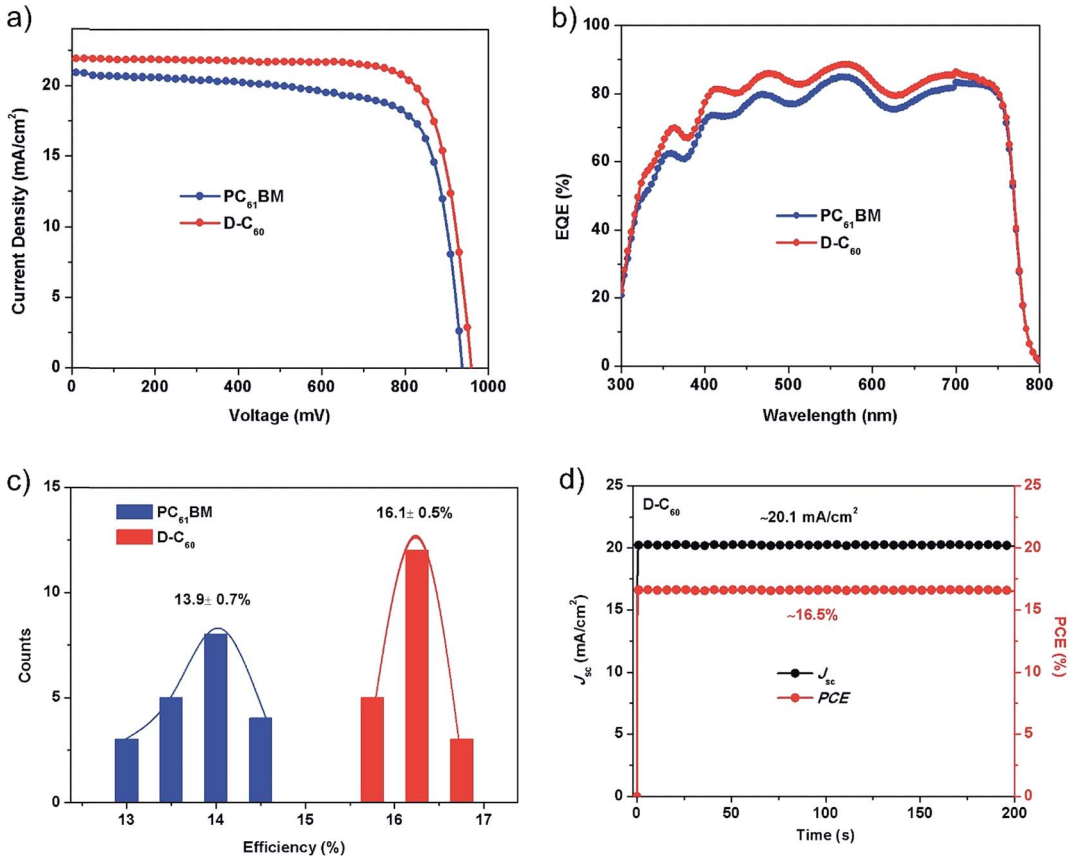

Fig. 3 Device performance and reproducibility of perovskite solar cells fabricated by using D-C_{60} and $PC_{61}BM$ as ETMs. (a) *J–V* curves of devices using D-C_{60} and $PC_{61}BM$. (b) EQE spectra for perovskite solar cells fabricated by using D-C_{60} and $PC_{61}BM$ as ETMs. (c) Histograms of device PCE measured for 20 individual devices based on $PC_{61}BM$ and D-C_{60} ETMs. (d) Maximal steady-state photocurrent output at the maximum power point for D-C_{60} based device at 0.82 V and its corresponding power output.

PEDOT:PSS layer, perovskite layer and fullerene derivative layer are around 40 nm, 350 nm and 60 nm, respectively.

The *J–V* curves of PSCs with $PC_{61}BM$ and D-C_{60} as the ETMs were obtained under AM 1.5G irradiation (100 mW cm^{-2}) in air. The *J–V* curves of the devices are shown in Fig. 3a and the key photovoltaic performance parameters V_{oc}, J_{sc}, FF, and PCE are listed in Table 2. The most efficient device using D-C_{60} as ETM yielded a PCE of 16.6%. The efficiencies are significantly higher than those of devices based on $PC_{61}BM$ as ETM, which resulted in an optimal PCE of 14.7%.

In order to better compare the device performances, a statistical histogram of the efficiencies of 20 individual devices using $PC_{61}BM$ and D-C_{60} as the ETMs are shown in Fig. 3c. The average efficiencies for D-C_{60} and $PC_{61}BM$ based devices are 16.1 ± 0.5% and 13.9 ± 0.7%, respectively. The narrower distribution of the key photovoltaic parameters illustrate that D-C_{60} is an excellent ETM for inverted planar structure PSCs.

The higher J_{sc} values of the D-C_{60} based devices were verified by the incident photon-to-electron conversion efficiency (IPCE) spectrum, as shown in Fig. 3b. The integrated current densities from the IPCE curve for devices involving D-C_{60} and $PC_{61}BM$ as the ETMs are 21.5 and 20.4 mA cm^{-2}, respectively, which are consistent with the values from the *J–V* curves. Furthermore, the higher J_{sc} and FF of D-C_{60} based devices can be related to the higher electron mobility and electron extraction ability.

The maximal steady-state power and photocurrent outputs were used to further verify device efficiencies. As shown in Fig. 3d, D-C_{60} based devices resulting in 20.1 mA cm^{-2} at 0.82 V had PCEs of 16.5%. $PC_{61}BM$ based devices resulting in 18.2 mA cm^{-2} at 0.80 V, had PCEs of 14.5% (Fig. S5†). Both efficiencies are very similar to the values determined from the *J–V* data.

It is worth noting that the D-C_{60} based devices exhibited a slightly higher V_{oc} than those of $PC_{61}BM$ based devices, which can be reasonably attributed to the slightly higher LUMO energy

Table 2 Summary of device performance analysis in Fig. 3. The calculated J_{sc} values are obtained from the EQE curves

Type	V_{oc} (V)	J_{sc} (mA cm^{-2})	Calculated J_{sc} (mA cm^{-2})	FF (%)	PCE (%)
$PC_{61}BM$	0.94	20.96	20.4	74.4	14.7
D-C_{60}	0.96	21.89	21.5	78.8	16.6

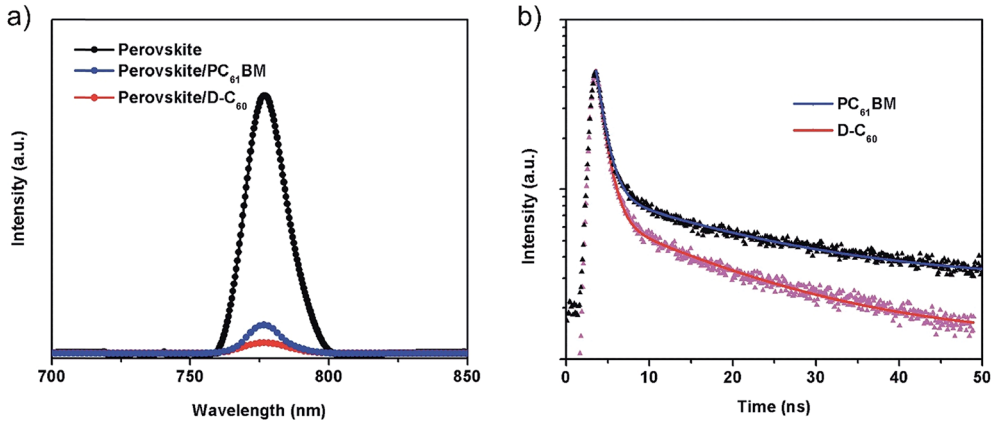

Fig. 4 (a) Steady-state photoluminescence spectra, and (b) TRPL decay transient spectra of FTO/perovskite/$PC_{61}BM$ and FTO/perovskite/D-C_{60}.

level of D-C_{60}.[36–38] The hysteresis effects of the devices were also studied. As shown in Fig. S6,† no obvious *J–V* curve differences were observed, regardless of the scan direction for the D-C_{60} based devices. The negligible hysteresis effect in the PSCs with D-C_{60} as the ETMs further indicate that the fullerene derivatives effectively passivate the charge traps at the fullerene/perovskite interface.[10,39]

To investigate the electron extraction ability of D-C_{60} as the ETM in PSCs, steady state and time-resolved photoluminescence (PL, TRPL) spectra were recorded. Fig. 4a shows the steady-state PL spectra of perovskite, perovskite/$PC_{61}BM$ and perovskite/D-C_{60} thin film substrates. When the perovskite layer forms a contact with $PC_{61}BM$ or D-C_{60}, a significant PL quenching effect was observed. Notably, devices based on D-C_{60} show more efficient PL quenching than those based on $PC_{61}BM$, which indicates that D-C_{60} inhibits electron–hole recombination more efficiently.[9] Additionally, TRPL, was measured by monitoring the emission peak of the perovskite layer as a function of time as shown in Fig. 4b. Perovskite/D-C_{60} devices exhibit a shorter PL decay time (11.1 ns) than that observed for the perovskite/$PC_{61}BM$ (14.0 ns) devices, which implies that electrons are more efficiently transferred to D-C_{60} than to $PC_{61}BM$. The faster decay is the result of PL quenching due to electron transfer at the interface, which suppresses electron–hole recombination and increases the J_{sc} and FF of the device.[40]

To probe charge transfer processes at the perovskite/D-C_{60} interface, electrical impedance spectroscopy (EIS) measurements were conducted for both perovskite/D-C_{60} and perovskite/$PC_{61}BM$ devices. The data were fit to a relatively simple equivalent circuit (Fig. S7 and Table S2†) consisting of a contact resistance between the fullerene/perovskite or perovskite/PEDOT:PSS interface and the recombination resistance (R_{rec}).[41] The Nyquist plots for the perovskite/D-C_{60} devices show lower contact resistances and larger recombination resistances than those for perovskite/$PC_{61}BM$ devices, thus D-C_{60} can decrease charge recombination more efficient than $PC_{61}BM$ at the fullerene/perovskite interface and electron extraction into the ETL is facilitated with D-C_{60}. This must be associated with the differences of charge recombination efficiencies at the perovskite/D-C_{60} or perovskite/$PC_{61}BM$ interface since the PEDOT:PSS/perovskite interface is identical for both cases.[42] This result is totally consistent with the higher PL quenching observed for perovskite/D-C_{60} devices.

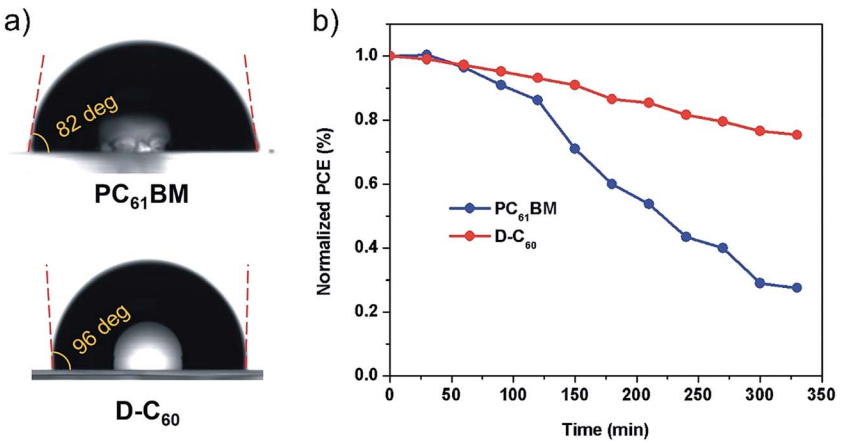

Fig. 5 (a) The images of the water droplet contact angles on different surfaces of fullerene derivative film. (b) Normalized PCE of perovskite solar cells employing D-C_{60} and $PC_{61}BM$ ETMs as a function of storage time in air.

Assessment of the stability of devices with D-C_{60} and $PC_{61}BM$ as the ETMs was conducted under a 50% humidity in air at room temperature without encapsulation. As shown in Fig. 5b, the devices with D-C_{60} retained more than 75% of its original performance after 10 days, while devices with $PC_{61}BM$ as the ETM retained only 25% after 10 days. The higher stability of the D-C_{60}-based devices may result from the higher hydrophobicity of D-C_{60} as well as the more compact self-assembled layer. As shown in Fig. 5a, the hydrophobic properties of the different fullerene derivatives were investigated. Water droplets on perovskite/$PC_{61}BM$ and perovskite/D-C_{60} layers result in contact angles of 82° and 96°, respectively. These values indicate that the two C_{60} subunits in D-C_{60} make the fullerene derivative more hydrophobic than $PC_{61}BM$.

4. Conclusions

In summary, we synthesized a dimeric fullerene derivative D-C_{60} and applied it as an ETM for PSCs taking advantage of its appropriate energy levels, relatively fast electron mobility, easy solution processability and device stability. As evidenced by CV, SCLC, EIS, PL and TRPL studies, D-C_{60} can effectively passivate the surface defects of the perovskite film, as well as efficiently extract and transport electrons. As a result, using D-C_{60} as ETM, PSC devices reached up to 16.6%, PCEs, higher than those of $PC_{61}BM$ based devices. Due to its higher hydrophobicity D-C_{60}, also enhanced the stability of the devices compared to $PC_{61}BM$. We believe that dimeric fullerene derivatives have the potential to become high performance alternatives for ETMs in PSCs.

Acknowledgements

L. E. thanks the US National Science Foundation (NSF) for generous support of this work under the NSF-PREM program (DMR 1205302) and the CHE-1408865. The Robert A. Welch Foundation is also gratefully acknowledged for an endowed chair to L. E. (Grant AH-0033).

References

1 A. Kojima, K. Teshima, Y. Shirai and T. Miyasaka, *J. Am. Chem. Soc.*, 2009, **131**, 6050–6051.
2 H. S. Kim, C. R. Lee, J. H. Im, K. B. Lee, T. Moehl, A. Marchioro, S. J. Moon, R. Humphry-Baker, J. H. Yum, J. E. Moser, M. Gratzel and N. G. Park, *Sci. Rep.*, 2012, **2**, 591–597.
3 G. Xing, N. Mathews, S. Sun, S. S. Lim, Y. M. Lam, M. Gratzel, S. Mhaisalkar and T. C. Sum, *Science*, 2013, **342**, 344–347.
4 S. D. Stranks, G. E. Eperon, G. Grancini, C. Menelaou, M. J. P. Alcocer, T. Leijtens, L. M. Herz, A. Petrozza and H. J. Snaith, *Science*, 2013, **342**, 341–344.
5 Q. Dong, Y. Fang, Y. Shao, P. Mulligan, J. Qiu, L. Cao and J. Huang, *Science*, 2015, **347**, 967–970.
6 C. Wehrenfennig, G. E. Eperon, M. B. Johnston, H. J. Snaith and L. M. Herz, *Adv. Mater.*, 2014, **26**, 1584–1589.
7 L. Q. Zhang, X. W. Zhang, Z. G. Yin, Q. Jiang, X. Liu, J. H. Meng, Y. J. Zhao and H. L. Wang, *J. Mater. Chem. A*, 2015, **3**, 12133–12138.
8 P. Docampo, J. M. Ball, M. Darwich, G. E. Eperon and H. J. Snaith, *Nat. Commun.*, 2013, **4**, 2761.
9 J. You, Z. Hong, Y. Yang, Q. Chen, M. Cai, T.-B. Song, C.-C. Chen, S. Lu, Y. Liu and H. Zhou, *ACS Nano*, 2014, **8**, 1674–1680.
10 Y. Shao, Z. Xiao, C. Bi, Y. Yuan and J. Huang, *Nat. Commun.*, 2014, **5**, 5784.
11 N.-G. Park, M. Grätzel, T. Miyasaka, K. Zhu and K. Emery, *Nature Energy*, 2016, **1**, 16152.
12 NREL, *Best Research-Cell Efficiencies*, 2016, http://www.nrel.gov/pv/assets/images/efficiency_chart.jpg.
13 J.-Y. Jeng, K.-C. Chen, T.-Y. Chiang, P.-Y. Lin, T.-D. Tsai, Y.-C. Chang, T.-F. Guo, P. Chen, T.-C. Wen and Y.-J. Hsu, *Adv. Mater.*, 2014, **26**, 4107–4113.
14 S. F. Volker, S. Collavini and J. L. Delgado, *ChemSusChem*, 2015, **8**, 3012–3028.
15 L. Meng, J. You, T.-F. Guo and Y. Yang, *Acc. Chem. Res.*, 2016, **49**, 155–165.
16 J.-Y. Jeng, Y.-F. Chiang, M.-H. Lee, S.-R. Peng, T.-F. Guo, P. Chen and T.-C. Wen, *Adv. Mater.*, 2013, **25**, 3727–3732.
17 W. Nie, H. Tsai, R. Asadpour, J.-C. Blancon, A. J. Neukirch, G. Gupta, J. J. Crochet, M. Chhowalla, S. Tretiak, M. A. Alam, H.-L. Wang and A. D. Mohite, *Science*, 2015, **347**, 522–525.
18 J. H. Heo, H. J. Han, D. Kim, T. K. Ahn and S. H. Im, *Energy Environ. Sci.*, 2015, **8**, 1602–1608.
19 Y. Shao, Y. Yuan and J. Huang, *Nat. Energy*, 2016, **1**, 15001.
20 J. H. Kim, S. T. Williams, N. Cho, C.-C. Chueh and A. K. Y. Jen, *Adv. Energy Mater.*, 2014, **5**, 1401229.
21 H. Azimi, T. Ameri, H. Zhang, Y. Hou, C. O. R. Quiroz, J. Min, M. Hu, Z.-G. Zhang, T. Przybilla, G. J. Matt, E. Spiecker, Y. Li and C. J. Brabec, *Adv. Energy Mater.*, 2015, **5**, 1401691–1401696.
22 X. Liu, W. Jiao, M. Lei, Y. Zhou, B. Song and Y. Li, *J. Mater. Chem. A*, 2015, **3**, 9278–9284.
23 X. Meng, Y. Bai, S. Xiao, T. Zhang, C. Hu, Y. Yang, X. Zheng and S. Yang, *Nano Energy*, 2016, **30**, 341–346.
24 X. Liu, F. Lin, C.-C. Chueh, Q. Chen, T. Zhao, P.-W. Liang, Z. Zhu, Y. Sun and A. K. Y. Jen, *Nano Energy*, 2016, **30**, 417–425.
25 Y. Xing, C. Sun, H. L. Yip, G. C. Bazan, F. Huang and Y. Cao, *Nano Energy*, 2016, **26**, 7–15.
26 J. Xie, X. Yu, X. Sun, J. Huang, Y. Zhang, M. Lei, K. Huang, D. Xu, Z. Tang, C. Cui and D. Yang, *Nano Energy*, 2016, **28**, 330–337.
27 C. Tian, E. Castro, T. Wang, G. Betancourt-Solis, G. Rodriguez and L. Echegoyen, *ACS Appl. Mater. Interfaces*, 2016, **8**, 31426–31432.
28 J. L. Delgado, E. Espíldora, M. Liedtke, A. Sperlich, D. Rauh, A. Baumann, C. Deibel, V. Dyakonov and N. Martín, *Chem.–Eur. J.*, 2009, **15**, 13474–13482.
29 J. Liu, X. Guo, Y. J. Qin, S. D. Liang, Z. X. Guo and Y. F. Li, *J. Mater. Chem.*, 2012, **22**, 1758–1761.

30 J. L. Segura, N. Martin and D. M. Guldi, *Chem. Soc. Rev.*, 2005, **34**, 31–47.
31 J. C. Hummelen, B. W. Knight, F. Lepeq, F. Wudl, J. Yao and C. L. Wilkins, *J. Org. Chem.*, 1995, **60**, 532–538.
32 H. Zhou, Q. Chen, G. Li, S. Luo, T. B. Song, H. S. Duan, Z. Hong, J. You, Y. Liu and Y. Yang, *Science*, 2014, **345**, 542–546.
33 Q. Chen, H. Zhou, Z. Hong, S. Luo, H.-S. Duan, H.-H. Wang, Y. Liu, G. Li and Y. Yang, *J. Am. Chem. Soc.*, 2014, **136**, 622–625.
34 Q. J. Sun, H. Q. Wang, C. H. Yang and Y. F. Li, *J. Mater. Chem.*, 2003, **13**, 800–806.
35 P. N. Murgatroyd, *J. Phys. D: Appl. Phys.*, 1970, **3**, 151–156.
36 L. Gil-Escrig, C. Momblona, M. Sessolo and H. J. Bolink, *J. Mater. Chem. A*, 2016, **4**, 3667–3672.
37 C.-G. Wu, C.-H. Chiang and S. H. Chang, *Nanoscale*, 2016, **8**, 4077–4085.
38 P.-W. Liang, C.-C. Chueh, S. T. Williams and A. K. Y. Jen, *Adv. Energy Mater.*, 2015, **5**, 1402321–1402327.
39 J. Xu, A. Buin, A. H. Ip, W. Li, O. Voznyy, R. Comin, M. Yuan, S. Jeon, Z. Ning, J. J. McDowell, P. Kanjanaboos, J.-P. Sun, X. Lan, L. N. Quan, D. H. Kim, I. G. Hill, P. Maksymovych and E. H. Sargent, *Nat. Commun.*, 2015, **6**, 7081.
40 P.-W. Liang, C.-Y. Liao, C.-C. Chueh, F. Zuo, S. T. Williams, X.-K. Xin, J. Lin and A. K. Y. Jen, *Adv. Mater.*, 2014, **26**, 3748–3754.
41 D. Liu, J. Yang and T. L. Kelly, *J. Am. Chem. Soc.*, 2014, **136**, 17116–17122.
42 A. Dualeh, T. Moehl, N. Tetreault, J. Teuscher, P. Gao, M. K. Nazeeruddin and M. Graetzel, *ACS Nano*, 2014, **8**, 362–373.

